35th Annual International Conference of the IEEE EMBS
Osaka, Japan, 3 - 7 July, 2013

Prior Knowledge Enhanced Random Walk for Lung Tumor Segmentation from Low-Contrast CT Images

Hui Cui, Xiuying Wang, Michael Fulham, David Dagan Feng

***Abstract*—The separation of a lung tumor from adjacent normal tissue, which has similar intensity values and indistinct boundaries on low-contrast CT images is a challenging task. In this paper, a prior knowledge enhanced random walk (RW) is proposed to account for the prior functional knowledge from PET and intensity information from CT. The prior knowledge acquired from PET is used for the automated selection of foreground seeds, defined as the tumor confidence region, the background seeds and the walking range to increase computational efficiency of the RW algorithm in CT. The tumor confidence region is also used for balancing transition, and thus limiting the information propagation range through a weight factor. The experimental evaluation on 18 low-contrast CT images with manual tumor segmentation demonstrated that our method outperformed RW and random walk from restart (RWR) as measured by the Dice similarity coefficient (DSC).**

I. Introduction

Lung cancer is a common cause of death and despite improvements in many aspects of modern medical care, the five-year survival rate remains poor at around 15% over the last few decades [1]. Early diagnosis, accurate staging and effective treatment of lung cancer are critical in improving survival. It has been suggested that if small non-small cell lung cancers (NSCLCs) can be removed prior to regional and more widespread dissemination the 5-year survival rate could be increased to approximately 80% [2].

Combined PET-CT scanners are now widely used in lung tumor diagnosis and treatment because they provide complementary functional information and anatomical information from a single scanning session. When radiotherapy is considered for treatment it is vital to delineate the tumor margins by segmentation to minimize damage to healthy tissues. Since CT provides better anatomical information and higher resolution than PET, tumor segmentation and delineation is mostly based on CT. However, to segment a tumor when it abuts or involves adjacent structures such as mediastinum and chest wall where there are similar intensities remains a challenging problem.

H. Cui is with the Biomedical and Multimedia Information Technology (BMIT) research group, School of Information Technologies, The University of Sydney, Australia (e-mail: hcui7511@uni.sydney.edu.au)

X. Wang is with the BMIT research group, School of Information Technologies, The University of Sydney, Australia (e-mail: xiuying@it.usyd.edu.au).

M. Fulham is with Faculty of Medicine, The University of Sydney and Department of PET and Nuclear Medicine, Royal Prince Alfred Hospital, Australia (e-mail: michael.fulham@sydney.edu.au).

D. D. Feng is with the BMIT research group, School of Information Technologies, The University of Sydney, Australia and Med-X Research Institute, Shanghai Jiao Tong University, China (e-mail: dagan.feng@sydney.edu.au).

Most lung tumors have high uptake of 18F-fluoro-deoxy-glucose (^{18}FDG), the most common PET tracer used in clinical medicine and characteristic is used to identify the tumors and their sites of spread. Recent work on PET lung tumor segmentation emphasized a fuzzy locally adaptive Bayesian algorithm [3] for heterogeneous tumor distribution [4] but there was no attention to tumor separation. In our previous work, a tumor-customized downhill (TCD) method was effective in the delineation and separation of tumors from adjacent neighbors with similar densities [5]. The segmentation accuracy was further improved by incorporating the standard uptake value (SUV) downhill feature into the energy function of graph cuts [6]. Other graph based methods including the random walk (RW) have been used for PET lung tumor segmentation [7].

Random walk has attracted increasing research attention due to its ability to segmenting an object with weak or indistinct boundaries [8]. Grady et al reported that RW was promising for the segmentation of lung tumors [9]; Chen et al [10] suggested that it was useful for malignant pleural mesothelioma from CT images. However, the segmentation results in RW are affected by the number and location of seeds. In addition, as Kim et al [11] indicate, RW only considers the local relationship between an un-labeled pixel and the border of the pre-labeled region, thus useful information of seeds inside the region is ignored. To solve this problem, Kim et al proposed random walk with restart (RWR) [11]; the RWR takes into account the across-the-board relationship between pixels and all possible paths between two nodes. These investigators reported that the RWR segmentation accuracy was improved by this approach.

The current RW-based segmentation mostly depends on interactive input of seeds, and works on a single image modality without helpful prior knowledge to improve the segmentation accuracy. In this paper we present a prior knowledge enhanced RWR method for lung tumor segmentation from CT that takes into account the enhanced confidence in tumor location provided by PET and the relatively clear boundary information from CT.

II. Methods

A. Problem definition and hypothesis

For a given image $I = \{x_1 \ldots \ldots \ldots$ and seed set $L = (L_1 \ldots \ldots \ldots$, the aim of segmentation is to group each unlabeled pixel $x_i \in I$ to L_k. The segmentation task can be solved by calculating the probability for each pixel to decide its membership.

While RWR [10] provides an effective solution to the probabilistic problem, our hypothesis is that the prior knowledge, such as the tumor confidence region extracted from PET, would help on deciding a pixel's membership, and hence would improve segmentation accuracy.

B. Related work

1) Random walk for image segmentation:

Given an image I, a weighted graph $G=(V,E)$ is defined with $v_i = x_i$, and the edges in set E are weighted according to weighted matrix W with entries $w_{ij} = \exp(-\|g_i - g_j\|^2 / \sigma)$. The state $\pi_{li}^{(t)}$ of a walker starting from a labeled pixel x_l and arrives at x_i after t steps can be formulated as equation (1)

$$\pi_{li}^{(t)} = \alpha\delta(i=l) + (1-\alpha)\sum_{x_j} \pi_{li}^{(t-1)} p_{ji} \quad (1)$$

where $\delta(rel)=1$ when rel is true and 0 otherwise. This means that when arriving at each pixel, if the pixel is labeled, the walker will go back to the starting seed x_l with a restart probability α, otherwise with the probability $1-\alpha$, the walker selects a neighbor pixel x_j with probability p_{ij} and moves to its neighbor. It is clear that if α increases, the probability that a random walker travels over a larger area decreases. With $\left[\mathbf{\Pi}^{(t)}\right]_{li} = \pi_{li}^{(t)}$, Equation (1) can be formulated as $\mathbf{\Pi}^{(t)} = \alpha\mathbf{I} + (1-\alpha)\mathbf{\Pi}^{(t-1)}\mathbf{P}$, where $\mathbf{P}$ is the transition matrix defined as $P_{ij} = w_{ij} / \sum_{\beta\in E(i)} w_{i\beta}$.

As random walk on edge-weighted graphs is a special case of Markov chain and at the steady state of the system $\mathbf{\Pi}^{(t)} = \mathbf{\Pi}^{(t-1)} \cdot \mathbf{P} = \mathbf{\Pi}^{(0)} \cdot \mathbf{P}^t$, thus

$$\mathbf{\Pi} = \alpha(\mathbf{I} - (1-\alpha)\mathbf{P})^{-1} \quad (2)$$

Finally the probability of pixel x_i belonging to label set L_k can be obtained by $\eta_i^k = [B\mathbf{\Pi}]_{ki}$, where B is defined as equation (3), Q_k is the set of seeds with label L_k.

$$[B]_{ki} = \begin{cases} \dfrac{1}{|Q_k|}, & \text{if } label(x_i) \in L_k \\ 0, & \text{otherwise} \end{cases} \quad (3)$$

2) Tumor-customized downhill for lung tumor segmentation from PET:

The Tumor-customized downhill (TCD) segmentation [5] starts from a voxel with SUV_{max} within the tumor region. During the irritation process, for each labeled voxel v_j, its neighboring voxels v_i are evaluated and labeled according to equation (4)

$$l_{v_i} = \begin{cases} 1, & SUV(v_i) \le SUV(v_j) \,\&\, nGM(v_i) \ge \phi(v_i) \\ 0, & \text{otherwise} \end{cases} \quad (4)$$

where $\phi(v_i) = \dfrac{1}{x_2 - x_1}(x_2 - nSUV(v_i))$ is the stopping criterion function. The two control points $x_1 = \min\{x_i \mid \varphi(x_i) = 0\}$ and $x_1 = \min\{x_i \mid \varphi(x_i) = 0\}$ are estimated based on the relationship of pairs of normalized SUV (nSUV) and normalized GM (nGM) using a second degree polynomial regression function $\varphi(x)$.

C. Prior knowledge enhanced RW

The overview of our proposed method is shown in Figure 1. The first step is to acquire the prior knowledge from the input PET images. After detecting the tumor confidence region, background seeds and the walking range on PET, the information is mapped back to the corresponding CT. Then the graph is modeled on CT to get the essential matrices for the computation of the steady-state probabilities for each pixel. Finally, the probability map and output tumor contour are obtained. There are two labels with $L_1 = L_R$ for the foreground and $L_2 = L_U$ for the background.

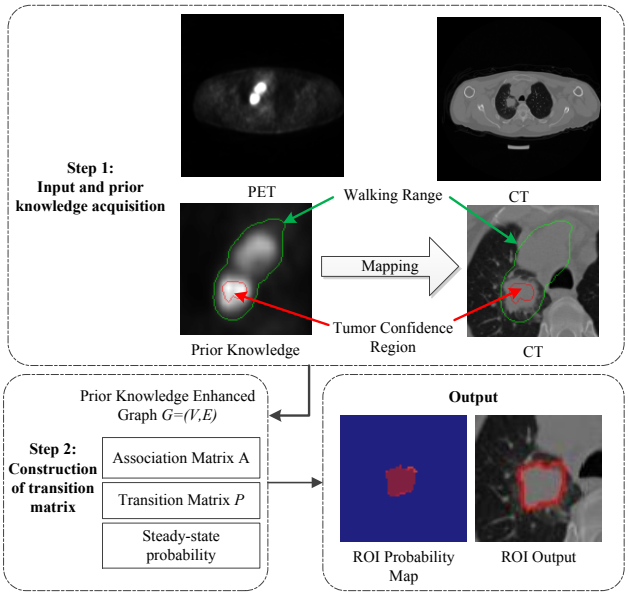

Figure 1. Framework of prior knowledge enhanced random walk

1) Prior knowledge from PET

Tumor confidence region definition: In clinical practice and as discussed by Boellaard [12], a region with 80% SUV_{max} in PET images is considered to belong to a tumor. In our method, the tumor confidence region Q_R is extracted automatically from PET by using TCD, which is able to separate the tumor from surrounding tissues where there is a high SUV e.g the heart. The tumor confidence region is then mapped onto CT and the corresponding pixels on CT are used as foreground seeds. Q_R also has effects on the association matrix A and the transition matrix P between two pixels by decreasing the weight of region outside Q_R.

Background seeds and walking range definition: The contour of 10% SUV_{max} extracted by TCD is mapped onto the CT image and used as background seeds labeled as L_U. In addition, the contour also serves as the walking range of the

random walker to limit the traveling range and hence to speed up the calculation.

2) Construction of transition matrix:

Since the higher the association possibility between a L_R candidate and Q_R is, the greater the transition probability that a random walker arrives at it. Therefore the nodes outside the tumor confidence region $Q_{uR} = I - Q_R$ are assigned a weight factor $\gamma \in (0,1)$, and the association matrix $\mathbf{A}$ between two nodes is defined as

$$a_{ij} = \begin{cases} 0, & v_i = v_j \\ 0, & v_i \neq v_j \ \& \ (v_i, v_j) \notin E \\ w_{ij}, & v_i \in Q_R \ \& \ (v_i, v_j) \in E \\ \gamma \cdot w_{ij}, & v_i \in Q_{uR} \ \& \ (v_i, v_j) \in E \end{cases} \quad (5)$$

Then the transition matrix $\mathbf{P} = [p_{ij}]_{n \times n}$ is obtained by row-normalized $\mathbf{A}$. However, after row normalization, the factor γ is lost. Therefore, when the matrix $\mathbf{P}$ is defined according to equation (6), the rows corresponding to Q_{uR} are multiplied by factor γ again. It is obvious that when γ increases from 0 towards 1, the impact of Q_R decreases. The value of γ is obtained by the training datasets.

$$\mathbf{P} = \mathbf{P}_R + \gamma \mathbf{P}_{uR} \quad (6)$$

Therefore, with the final state reformulated according to Equation (2), the probability $\eta_i^k = [B\mathbf{\Pi}]_{ki}$ is obtained where

$$\mathbf{\Pi} = \alpha(\mathbf{I} - (1-\alpha)\mathbf{P}_R - \gamma(1-\alpha)\mathbf{P}_{uR})^{-1} \quad (7)$$

Finally, by assigning the decision rule $R_i = \arg\max_{L_k} \eta_i^k$ to each pixel x_i, the segmentation result is obtained.

An overview of the prior knowledge enhanced graph construction process and the different transition states for Q_R and Q_{uR} at time $t+1$ are illustrated in Figure 2.

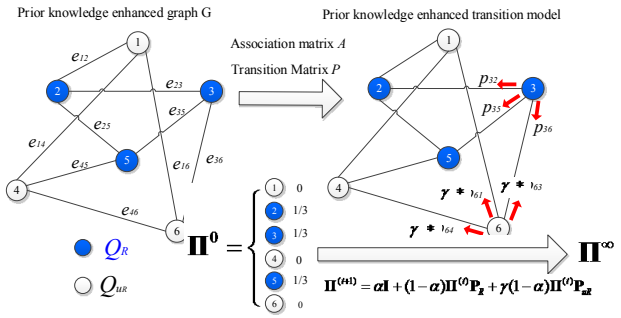

Figure 2. Illustration of the construction of the transition matrix. Blue labels indicating the tumor confidence region Q_R while white labels indicating Q_{uR}.

III. Experimental Evaluation

A. Clinical data

We used 20 PET-CT NSCLC cases including ten simple cases, where the tumor was located in the lung parenchyma but with no involvement of adjacent structures; all with ground truth (GT) i.e pathological confirmation; eight out of ten complicated cases with GT. The complicated cases included five with chest wall involvement; three with involvement of the mediastinum and two where the tumor was attached to the chest wall and the mediastinum. These studies are from a Biograph True V 64-slice PET-CT scanner (Siemens Medical Solutions). The CT scans were reconstructed using a matrix of 512 × 512 pixels with pixel size of 0.98 mm × 0.98 mm × 2 mm. The PET scans were reconstructed using a matrix of 168 × 168 pixels with pixel size of 4.07 mm × 4.07 mm × 2 mm. The PET volumes are registered to the corresponding CT volumes based on the affine transformation from Insight Toolkit (ITK).

The proposed method was performed on 2D images and conducted by using MATLAB R2010b on the processor with Core i5-2400 CPU @ 3.10GHz, installed memory (RAM) 4.00GB.

B. Experimental results and Discussion

1) Parameters Selection

There were two free parameters in our model. For the restarting probability α, we set the same value with RWR [10] for comparison.

The selection of the association weight factor γ was based on the training of 18 cases with GT, by verifying the values of γ from 0.35 to 0.9 and the higher the value is, the less the PET prior would be considered. The accuracy was measured by average Dice similarity coefficient (DSC) of the segmentation on CT with manually selected foreground and background seeds. As shown in Figure 3, when γ was around 0.65 (marked as red spot), the segmentation was stable and reached high accuracy. Therefore, γ was set as 0.65 in our experiments.

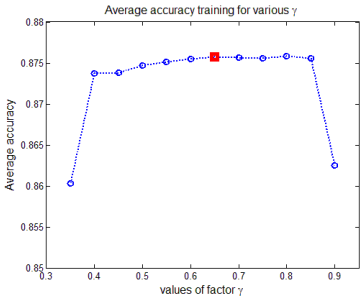

Figure 3. Parameter γ value selection

2) Quantitative validation

The segmentation results of the three methods were compared (see Figure 4) including 8 complicated cases shown case by case, average DSC for the 10 simple cases and for the overall cases. Compared with RW, the RWR produced slightly improved overall segmentation accuracy for the CT, which was mainly because the texture information of the foreground seeds was not sufficient when compared with the natural images in [11]. For the simple cases, RW outperformed RWR because the walking range for RWR was

too large. The PKE-RW outperformed RWR due to the prior tumor related information from PET.

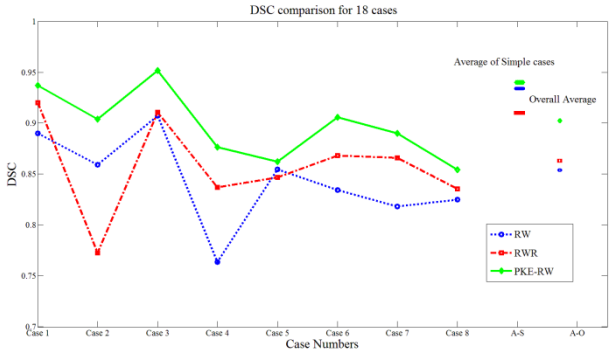

Figure 4. DSC comparison of RW, RWR and PKE-RW. Cases 1-8 indicate the complicated cases, A-S is the average DSC of the 10 simple cases and A-O is the average of the overall 18 cases

Furthermore, because our method limited the walking range, the walker would not travel around the whole image, and thus our PKE-RW, on average, used 1.56 seconds for segmentation when compared to 4.36 seconds for RWR. RW took the shortest average time, 1.49 seconds, because the graph is four-connected.

3) Qualitative Validation

The segmentation results for the complicated cases including Case 1 in Figure 4 where tumor is adjacent to the mediastinum (see Figure 5), Case 2 and Case 3 in Figure 4 where the tumors are attached to chest wall (as shown in Figure 6) and Case 4 where tumor is adjacent to/involves the mediastinum and the chest wall (see Figure 7).

RW RWR PKE-RW GT

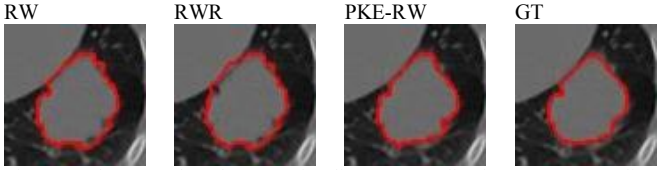

Figure 5. The case when the tumor is adjacent to mediastinum, corresponding to case 1 in Figure 4.

RW RWR PKE-RW GT

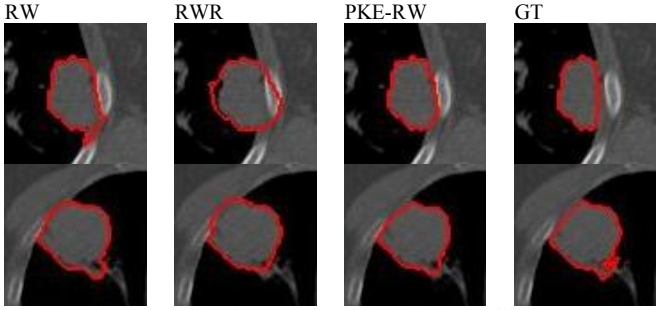

Figure 6. The cases when the tumor involves the chest wall. First row is case 2 and second row is case 3 in Figure 4.

RW RWR PKW-RW GT

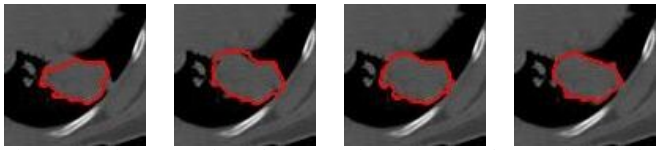

Figure 7. The case when the tumor involves the chest wall and the mediastinum. Corresponding to case 4 in Figure 4.

IV. Conclusion

We present an enhanced RW model that fully utilizes the prior knowledge on PET for lung tumor segmentation from low-contrast CT. The influence of the tumor confidence region and the walking range were used and the foreground and background seeds were obtained based on the PET automatically. Our results show that segmentation accuracy and speed were improved.

References

[1] F. B. Ahmedin Jemal, Melissa M. Center, Jacques Ferlay, Elizabeth Ward and David Forman, "Global cancer satatistics," *CA: A Cancer Journal for Clinicians,* vol. 61, pp. 69-90, 2011.

[2] *Lung cancer: what you need to know*. Available: http://www.mydr.com.au/cancer-care/lung-cancer-what-you-need-to-know

[3] M. Hatt, C. C. le Rest, P. Descourt, A. Dekker, D. De Ruysscher, M. Oellers, P. Lambin, O. Pradier, and D. Visvikis, "Accurate Automatic Delineation of Heterogeneous Functional Volumes in Positron Emission Temography for Oncology Applications," *International Journal of Radiation Oncology Biology Physics,* vol. 77, pp. 301-308, May 1 2010.

[4] M. Hatt, C. C. Le Rest, N. Albarghach, O. Pradier, and D. Visvikis, "PET functional volume delineation: a robustness and repeatability study," *European Journal of Nuclear Medicine and Molecular Imaging,* vol. 38, pp. 663-672, Apr 2011.

[5] C. Ballangan, X. Wang, M. Fulham, S. Eberl, Y. Yin, and D. Feng, "Automated Delineation of Lung Tumors in PET Images Based on Monotonicity and a Tumor-Customized Criterion," *IEEE Transactions on Information Technology in Biomedicine,* vol. 15, pp. 691-702, 2011 2011.

[6] C. Ballangan, X. Wang, M. Fulham, S. Eberl, and D. D. Feng, "Lung tumor segmentation in PET images using graph cuts," *Computer Methods and Programs in Biomedicine*. http://dx.doi.org/10.1016/j.cmpb.2012.10.009

[7] D. P. Onoma, S. Ruan, I. Gardin, G. A. Monnehan, R. Modzelewski, and P. Vera, "3D random walk based segmentation for lung tumor delineation in PET imaging," in *IEEE International Symposium on Biomedical Imaging*, 2012, pp. 1260-1263.

[8] L. Grady, "Random walks for image segmentation," *IEEE Transactions on Pattern Analysis and Machine Intelligence,* vol. 28, pp. 1768-1783, Nov 2006.

[9] L. Grady, T. Schiwietz, S. Aharon, and M. Westermann, "Random walks for interactive organ segmentation in two and three dimensions: Implementation and validation," in *Medical Image Computing and Computer-Assisted Intervention - Miccai 2005, Pt 2*. vol. 3750, J. S. G. G. Duncan, Ed., ed, 2005, pp. 773-780.

[10] M. Chen, E. Helm, N. Joshi, S. M. Brady, and Ieee, "Random Walk-based Automated Segmentation For The Prognosis of Malignant Pleural Mesothelioma," in *2011 8th IEEE International Symposium on Biomedical Imaging: From Nano to Macro*, ed, 2011, pp. 1978-1981.

[11] T. H. Kim, K. M. Lee, and S. U. Lee, "Generative Image Segmentation Using Random Walks with Restart," in *Proceedings of the 10th European Conference on Computer Vision: Part III*, Marseille, France, 2008, pp. 264-275.

[12] R. Boellaard, "Mutatis Mutandis: Harmonize the Standard!," *Journal of Nuclear Medicine,* vol. 53, pp. 1-3, Jan 1 2012.